Semiconductor Physics, Quantum Electronics & Optoelectronics, 2021. V. 24, No 2. P. 192-199.

Optoelectronics and optoelectronic devices

Simulation analysis to optimize the performance of homojunction *p-i-n* $In_{0.7}Ga_{0.3}N$ solar cell

S. Hussain, Md. T. Prodhan and Md. M. Rahman

Department of Electrical and Electronic Engineering, University of Dhaka, Dhaka-1000, Bangladesh
Corresponding author e-mail: sakhawat@du.ac.bd, Mobile: +8801716865552

Abstract. Simulation analysis has been carried out to determine the perfect structural parameters of homojunction *p-i-n* $In_{0.7}Ga_{0.3}N$ solar cell to obtain maximum overall efficiency. It has been demonstrated that *n*-layer of 16-nm, intrinsic layer (*i*-layer) of 0.5-μm and *p*-layer of 3-μm thickness with specific doping concentrations of $1\cdot10^{20}$ cm^{-3} for *n*-layer and $1\cdot10^{18}$ cm^{-3} for *p*-layer allow us to achieve the maximum efficiency 29.21%. The solar cell structure provides an open circuit voltage of 1.0 V, short circuit current density of 33.15 mA/cm^2 and the percentage of fill factor value of 88.03%. However, the efficiency drops drastically, if the dislocation density in *i*-layer is higher than $1\cdot10^{14}$ cm^{-3}, and unintentional doping concentration within *i*-layer is beyond $1.5\cdot10^{16}$ cm^{-3} of the structure.

Keywords: InGaN, homojunction, *p-i-n* solar cell, solar cell capacitance simulator (SCAPS).

https://doi.org/10.15407/spqeo24.02.192
PACS 85.60.Jb, 85.35.Be

Manuscript received 23.02.21; revised version received 27.03.21; accepted for publication 02.06.21; published online 16.06.21.

1. Introduction

The group III-nitride is a promising material system for optoelectronic application due to its ability to cover the solar spectrum from ultraviolet (3.51 eV) to infrared (0.78 eV) by bandgap engineering, which depends on the percentage of indium composition within the material [1–3]. Furthermore, its other properties such as high mobility, high saturation velocity, high absorption coefficient, radiation coefficient and low effective mass of electrons and holes, makes it to be an interesting material to study for solar cell application [4, 5]. In spite of having other materials such as Si, CdTe, $Cu(In,Ga)Se_2$ (CIGS), Cu_2ZnSnS_4 (CZTS) and organic resources for solar materials [6, 7], recently, huge research interest has been focused on InGaN materials, since it is more robust to solar radiation [8] and less toxic to environment than its counterparts [9].

On the other hand, incorporation of In into an epilayer of heterojunction solar cell introduces misfit dislocations and stacking faults at the interface due to lattice mismatch and also consists of *V*-defects, threading dislocations within the InGaN epilayer, which act as a recombination centers for charge carriers [10–12]. Moreover, the heterojunction InGaN has built in piezoelectric and spontaneous polarization [13] effects at the interface of the layers, which also play an important role at the overall efficiency of the solar cell [14, 15]. To overcome these detrimental effects, researchers are proposing to have nanopatterned sapphire [16] to reduce the overall dislocation density and also multi quantum well [17], superlattice structure [18], wide bandgap top cell of InGaN layer or even bounded hybrid multi junction for efficient solar cells [19, 20]. One can also construct a homojunction, strain free InGaN *p-i-n* solar structure to avoid the piezoelectric polarization effect within the active layer of the solar cell structure [21]. Using both MBE [22, 23] and MOCVD [24] growth techniques, researchers are trying to fabricate *p-i-n* homojunction solar cell of InGaN material with different percentage of In composition and layer thicknesses but find insignificant performance mainly due to material defects.

In this work, we have considered a homojunction *p-i-n* solar cell of $In_{0.7}Ga_{0.3}N$ material and try to simulate and identify the impacts of different layer thicknesses, pre-existing dislocation density within different layers and doping concentration of *p-i-n* layers to have a perfect structure for high efficiency solar cell. The numerical simulation package, solar cell capacitance simulator (SCAPS) [25], has been used to find out the open circuit voltage (V_{OC}), short circuit current density (J_{SC}), percentage of fill factor (% FF) and overall efficiency (% η) of the solar cell to propose the optimum solar cell structure.

2. Numerical simulation and device parameter

SCAPS-1D is a one-dimensional solar cell simulator developed at the Department of Electronic and Information Systems (EIS), University of Gent, Belgium. It can be used to numerically analyze the solar cell of several layers after giving some basic physical properties, namely: band gap, electron affinity, relative dielectric permittivity of the material, the conduction and valence band effective density of states of each layer and also the thermal velocity, mobility and effective mass of both electron and hole for the respective layers. Moreover, it allows the user to set layer thicknesses, contact layer properties, layer's donor and/or acceptor concentration values and their doping profile. One can incorporate the band-to-band recombination mechanism by introducing the radiative recombination coefficient, Auger electron and hole capture coefficients, Shockley–Read–Hall (SRH) recombination coefficient values and defect density within the layer to model the device more precisely.

In our work, as we have considered the homojunction $In_{0.7}Ga_{0.3}N$ *p-i-n* solar cell structure, we have determine the above mentioned physical properties for the system using the standard Vegard law in the following form:

$$Y(\mathrm{In_xGa_{1-x}N}) = Y(\mathrm{InN})x + Y(\mathrm{GaN})(1-x) - bx(1-x), \quad (1)$$

where x is the percentage of indium composition (x = 0.70 in our case), Y(InN) and Y(GaN) are the parameters for both InN and GaN system at room temperature (T = 300 K), b is the bowing parameter (for InGaN system, b = 140 [1]), which is used to calculate the band gap energy, and for other physical parameters it is zero.

The Caughey–Thomas approximation is employed for the electron mobility value as a function of carrier density [26]:

$$\mu(N) = \mu_{\min} + \frac{\mu_{\max} - \mu_{\min}}{1 + \left(\frac{N}{N_{ref}}\right)^{\alpha}}, \quad (2)$$

where the value of N_{ref} is $1\cdot10^{17}$ cm^{-3}, the values of μ_{min}, μ_{max} and α along with other parameters for $In_{0.7}Ga_{0.3}N$ system are listed in Table 1 by using Eq. (1) where necessary.

To simulate, we considered the initial cell structure shown in Fig. 1 below. The band-to-band recombination feature was added by considering the radiative recombination coefficient, Auger electron and hole capture coefficient values for the system. The initial structure parameters are listed in Table 2. Now, to find out the optimum device structure, we changed the layer thickness value, doping concentration and pre-existing dislocation density of different $In_{0.7}Ga_{0.3}N$ layers. While changing one particular parameter, for example *p*-layer thickness, we kept other parameters fixed at their initial or optimum values. Thus, we tried to find out the impacts of each parameter and analyzed the data to identify why such affects occur and how to achieve the highest efficiency from the solar cell.

3. Result and discussion

After putting all the physical parameters and the structural parameter values from Tables 1 and 2 for $In_{0.7}Ga_{0.3}N$ *p-i-n* solar cell into the SCAPS-1D simulator, we obtained the open circuit voltage (V_{OC}), short circuit current density (J_{SC}), percentage of fill factor (% FF) and the percentage of overall efficiency (% η) of our initial solar cell as 0.91 V, 32.86 mA/cm^2, 84.67% and 25.32%, respectively.

Table 1. Material parameters of InN, GaN and $In_{0.7}Ga_{0.3}N$ collected from literature and obtained using Eq. (1).

Parameter	InN	GaN	$In_{0.7}Ga_{0.3}N$	Reference
Bandgap (eV)	0.78	3.51	1.305	[1]
Electron affinity (eV)	5.6	4.2	5.18	[27]
Relative dielectric permittivity (ε_r)	10.5	8.9	10.02	[27]
Conduction band effective density of states (cm^{-3})	$8\cdot10^{17}$	$2\cdot10^{17}$	$6.2\cdot10^{17}$	[27]
Valence band effective density of states (cm^{-3})	$3\cdot10^{17}$	$3\cdot10^{17}$	$3\cdot10^{17}$	[27]
Electron and hole thermal velocity (cm/s)	$1\cdot10^{7}$	$1\cdot10^{7}$	$1\cdot10^{7}$	
μ_{min}	3138	1461	2634.9	[4, 26]
μ_{max}	774	295	630.3	[4, 26]
α	0.68	0.66	0.674	[4, 26]
Electron mobility (cm^2/(V·s))	3138 (when doping is $1\cdot10^{17}$)	1462 (when doping is $1\cdot10^{17}$)	2635–2740 (depending on doping from $1\cdot10^{17}$ to $1\cdot10^{20}$)	Using Eq. (2)
Hole mobility (cm^2/(V·s))	340	170	289	[27]
Effective mass of electrons	0.07	0.2	0.109	[1]
Effective mass of holes	0.6	1.25	0.795	[1]

Table 2. Structural parameter values for initial solar cell.	
Structural parameter	Values
n-layer thickness	6 nm
i-layer thickness	2 μm
p-layer thickness	2 μm
Donor doping concentration in *n*-layer, N_D	$1 \cdot 10^{18}$ cm^{-3}
Unintentional doping in *i*-layer	$1.5 \cdot 10^{15}$ cm^{-3}
Acceptor doping concentration in *p*-layer, N_A	$1 \cdot 10^{18}$ cm^{-3}
Pre-existing defect density, N_t	$1 \cdot 10^{14}$ cm^{-3}
Radiative recombination coefficient, *B* [28]	$7.5 \cdot 10^{-10}$ cm^3/s
Auger electron and hole capture coefficients, C_n and C_p [29]	$1.4 \cdot 10^{-30}$ cm^6/s
Electron and hole minority carrier lifetime, τ_n and τ_p	1 ns
For ohmic contact, metal contact	Nickel

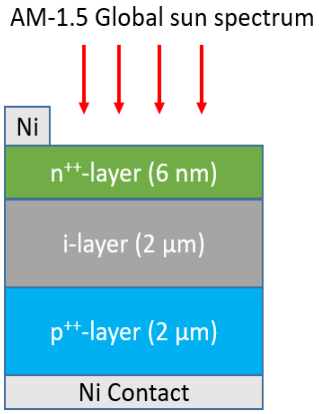

Fig. 1. Schematic $In_{0.7}Ga_{0.3}N$ *p-i-n* solar cell structure with initial layer thicknesses.

We then started changing the thickness of individual layers one-by-one and keeping other parameters fixed to their initial values or to the optimum values from the previous result. For example, we found that increasing the *n*-layer thickness from 6 up to 16 nm allow us to increase the overall efficiency from 25.32% up to 25.55%. However, beyond the 16-nm thickness of *n*-layer, the efficiency started to decrease as shown in Fig. 2a. The open circuit voltage and short circuit current density as a function of *n*-layer thickness is shown in Fig. 2b, where it is obvious that increasing the *n*-layer thickness reduces the J_{SC} term due to minority hole carrier recombination within the short neutral region but increases V_{OC} of the device. Thus, we obtained that the optimum *n*-layer thickness should be 16 nm. We kept the *n*-layer thickness as 16 nm for the rest of our analysis.

Considering the intrinsic layer thickness, we simulated the devices by setting the layer thickness from 0.1 to 2 μm, while keeping the other parameters fixed. The obtained results are shown in Fig. 3. Fig. 3a shows the relationship of open circuit voltage and short circuit current density, Fig. 3b shows relationship of fill factor and efficiency as a function of *i*-layer thickness variation. From the both graphs, it is obvious that *i*-layer of 0.5 μm performs the best, as the short circuit current density (J_{SC}), the percentage of overall efficiency (% η) and fill factor (% FF) are the highest ones: 33.23 mA/cm^2, 26.34% and 86.24%, respectively. However, the change in V_{OC} (in Fig. 3a) is insignificant as the change is very small (in the fourth decimal point).

To find out the impact of *p*-layer thickness on device performances, we simulated the device by keeping the *n*-layer and *i*-layer as 16 nm and 0.5 μm, respectively, and other parameters at their initial values. Fig. 4 shows the plot of the obtained data.

From Fig. 4, one can find that when increasing the *p*-layer thickness from 0.1 to 5 μm, the open circuit voltage, short circuit current density (Fig. 4a) and the percentage of overall efficiency (Fig. 4b) increase exponentially and get almost saturated at 3 μm. However, the percentage of fill factor (% FF) gets its highest value 86.31% at 0.5 μm and then starts to decrease and become almost fixed at 86.22% beyond the thickness of 2.5 μm (Fig. 4b). Thus, we have considered the best thickness for *p*-layer to be close to 3 μm.

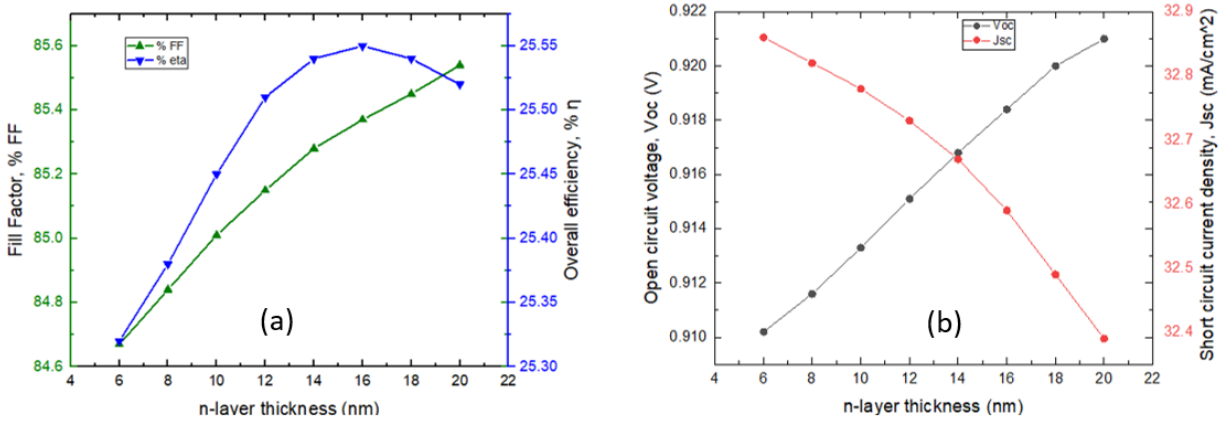

Fig. 2. Variation of percentage of fill factor and overall efficiency (a) and of V_{OC} and J_{SC} (b) as a function of *n*-layer thickness.

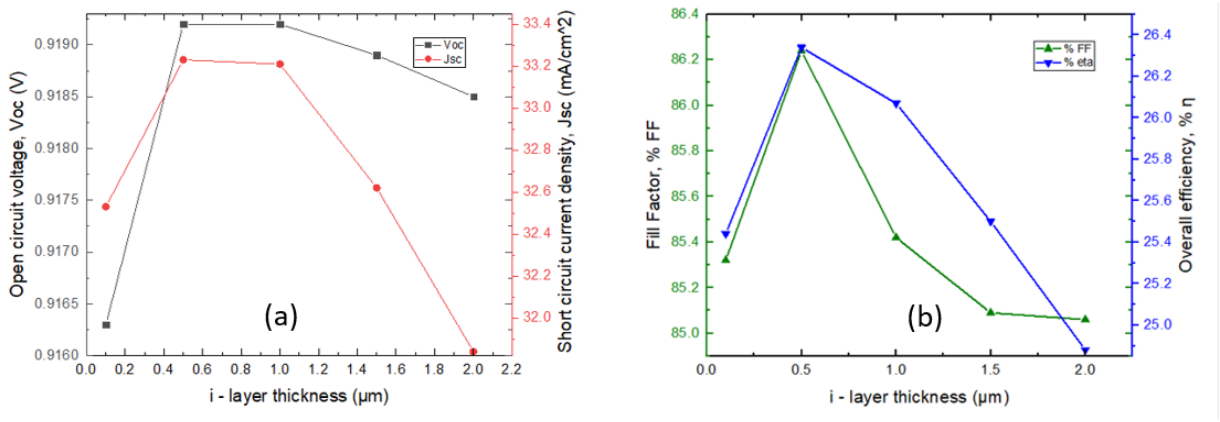

Fig. 3. Variation of V_{OC} and J_{SC} (a) and of fill factor and efficiency (b) as a function of *i*-layer thickness.

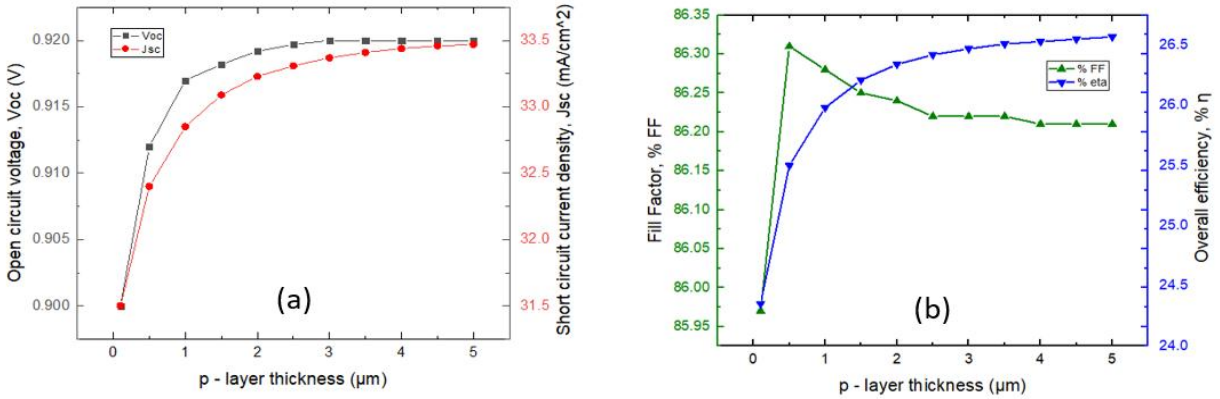

Fig. 4. Variation of V_{OC} and J_{SC} (a) and of fill factor and efficiency (b) as a function of *p*-layer thickness.

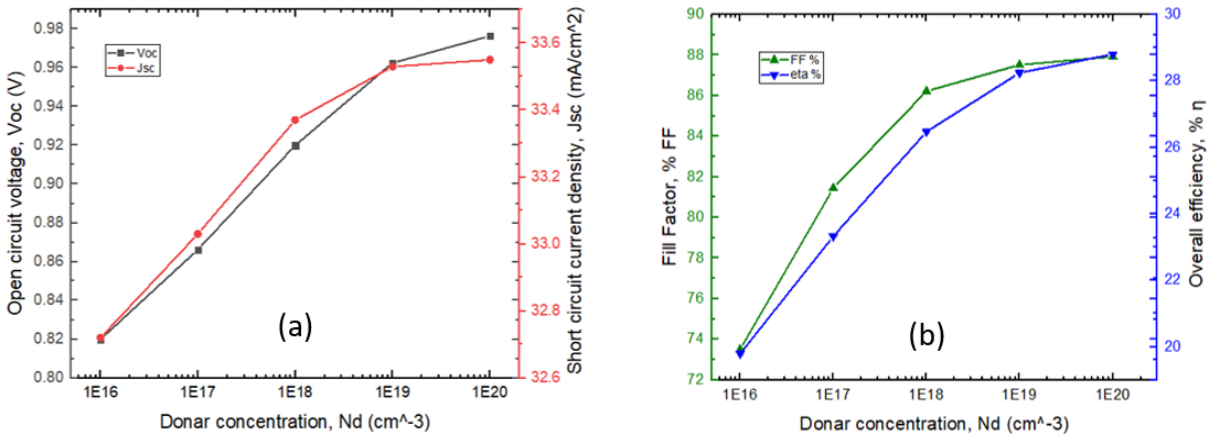

Fig. 5. Variation of V_{OC} and J_{SC} (a) and percentage of fill factor (% FF) and overall efficiency (% η) (b) as a function of donor concentration N_D (cm^{-3}).

Now, to see the impact of doping concentration, we modeled our structure with doping concentration from $1 \cdot 10^{16}$ to $1 \cdot 10^{20}$ cm^{-3} for *p*- and *n*-layer of the structure separately, while making the layer thicknesses of 16 nm, 0.5 μm and 3 μm for *n*-, *i*-, *p*-layers, respectively, and keeping the other parameters as shown in Tables 1 and 2. Figs 5 and 6 show the obtained data for *n*-layer doping and *p*-layer doping, respectively.

Fig. 5 suggests that all the output parameters, *i.e.*, open circuit voltage, short circuit current (Fig. 5a), percentage of fill factor and overall efficiency (Fig. 5b) of the solar cell, increase almost exponentially and get saturated at or near the donor doping concentration (N_D) close to $1 \cdot 10^{20}$ cm^{-3}. For example, the open circuit voltage (V_{OC}) is 0.97 V, short circuit current density (J_{SC}) is 33.55 mA/cm^2 and percentage of fill factor (% FF) is

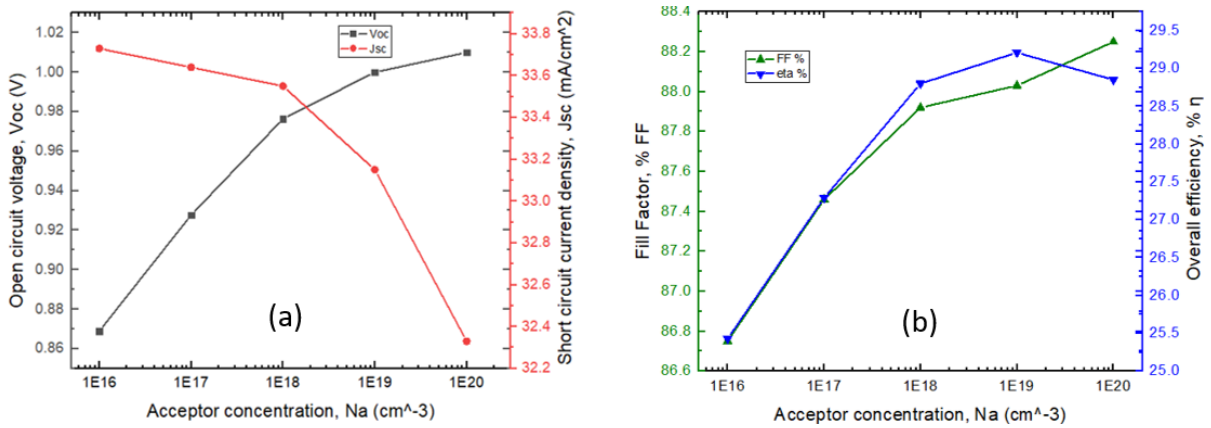

Fig. 6. Variation of V_{OC} and J_{SC} (a) and percentage of fill factor (% FF) and overall efficiency (% η) (b) as a function of acceptor concentration N_A (cm^{-3}).

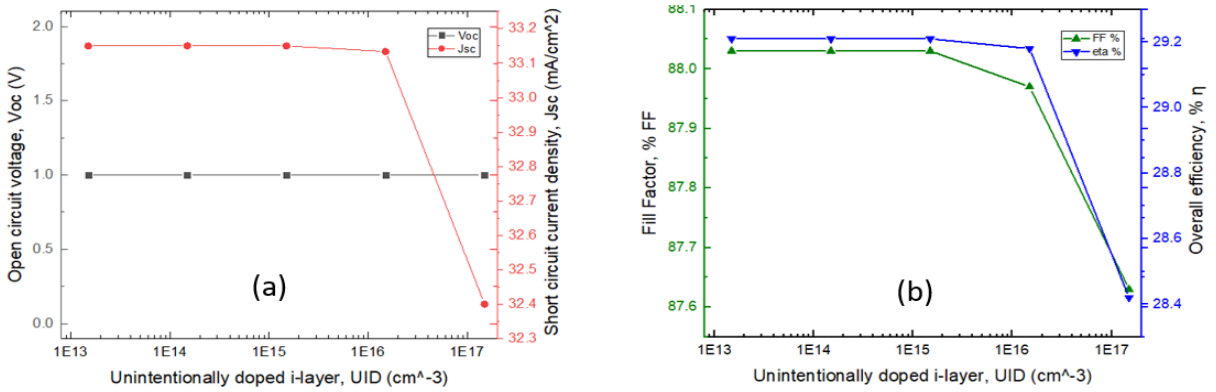

Fig. 7. Variation of V_{OC} and J_{SC} (a) and percentage of fill factor (% FF) and overall efficiency (% η) (b) as a function of unintentional doping concentration of intrinsic layer (cm^{-3}).

87.92%, while the overall efficiency (% η) is 28.80% at doping concentration of $1\cdot10^{20}$ cm^{-3}. Moreover, at that high doping concentration ($1\cdot10^{20}$ cm^{-3}) the $In_{0.7}Ga_{0.3}N$ *n*-layer will become degenerated material, as the Fermi level will be within the conduction band (141.5 meV from the lowest conduction band energy), which will help to make an ohmic contact with Ni metal for external connection.

In Fig. 6, we have presented the variation of open circuit voltage, short circuit current density, percentage of fill factor and the overall efficiency as a function of *p*-layer acceptor doping concentration N_A (cm^{-3}). From Fig. 6a, we have found that the short circuit current density decreases sharply after the acceptor concentration close to $1\cdot10^{18}$ cm^{-3}. But the other parameters increase as that of *n*-layer donor concentration variation. As it is always required to have higher short circuit current density from a solar cell, thus it is better to compromise open circuit voltage, percentage of fill factor and efficiency values slightly as shown in Fig. 6 to get the highest value of J_{SC} 33.55 mA/cm^2.

In the case of intrinsic layer (*i*-layer), it has been reported that when growing the InGaN layer, it generally gets unintentionally doped (UID) with donor type impurities of $5\cdot10^{16}$ cm^{-3} due to oxygen doping (as known shallow donor in GaN) [30]. However, we come to know from our simulation result (as shown in Fig. 7) that if we allow this amount of UID *i*-layer, the efficiency of the solar cell drops drastically. This takes place probably because some additional energy states appear within the band gap of the layer, which is caused by a high concentration of impurities, which act as a recombination centers for the generated electron-hole pair within the *i*-layer. Fig. 7a shows that the short circuit current density decreases from 33.15 mA/cm^2 down to 32.40 mA/cm^2, while the UID concentration is increased from $1.5\cdot10^{15}$ cm^{-3} up to $1.5\cdot10^{17}$ cm^{-3}. But if we could make the UID concentration below $1.5\cdot10^{15}$ cm^{-3}, then the short circuit current density (J_{SC}), percentage of fill factor (% FF) and overall efficiency (% η) are almost fixed at 33.15 mA/cm^2, 88.03% and 29.21%, respectively. However, the open circuit voltage value does not have any impact caused by the change in UID concentration and remains fixed at 1.0 V.

Finally, pre-existing dislocation density (N_t) within the InGaN layer is an important issue to deal with for efficient solar cell. We analyzed our structure when introducing the dislocation density from $1\cdot10^{14}$ up to $1\cdot10^{19}$ cm^{-3} for individual layers to identify the dependence of overall efficiency with respect to each layer's dislocation density values. Later, we also considered the dislocation density to be equal in all layers.

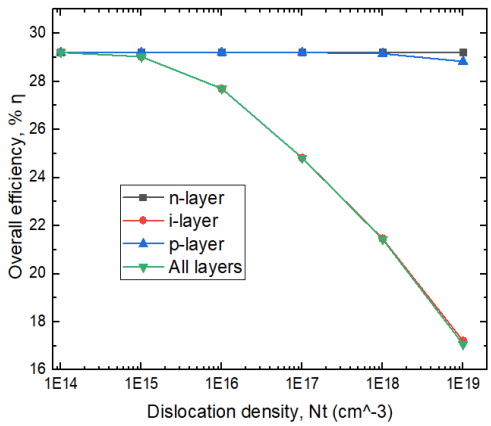

Fig. 8. Percentage of overall efficiency (% η) variation as a function of dislocation density N_t in individual layers and in the cell, respectively. (Color online.)

Fig. 8 shows the obtained result. It is important to note that dislocation density variation within *n*- and *p*-layer do not have significant impact on percentage of overall efficiency loss, as it is almost fixed at 29.21% (black (■) and blue (▲) lines in Fig. 8). But dislocation density variation within intrinsic layer (*i*-layer) has a huge impact on the percentage of overall efficiency (% η), because the efficiency drops dramatically from 29.21% to 17.21%, when the dislocation density (N_t) varies from $1\cdot10^{14}$ cm^{-3} up to $1\cdot10^{19}$ cm^{-3} as shown by red (●) line in Fig. 8. Moreover, while considering the dislocation density to be equal in all the layers (green (▼) line), it follows that the exact percentage of overall efficiency (% η) values reaches that of *i*-layer plot (red line). Thus, it is obvious that the *i*-layer should have as low dislocation density as $1\cdot10^{14}$ cm^{-3} to get an effective solar cell structure.

The results show that a high quality, strain free and less dislocation density ($\leq 1\cdot10^{14}$ cm^{-3}) $In_{0.7}Ga_{0.3}N$ alloy is a key element to achieve high efficient homojunction *p*-*i*-*n* solar cell structure. In the near future, fabrication of such alloy will be the main challenge to overcome. Again the voltage and current leakage parameters such as series and shunt resistance, as well as decreasing light absorption coefficient (due to air-semiconductor light propagation) of the device should be minimized to get an efficient group III-nitride material based solar cell.

4. Conclusion

In this work, we simulate a homojunction *p*-*i*-*n* solar cell of group III-nitride material using SCAPS simulation software. We come to know that if we have a high quality, strain free and less defect density ($\leq 1\cdot10^{14}$ cm^{-3}) $In_{0.7}Ga_{0.3}N$ alloy, then we can easily design a solar cell structure to get an overall efficiency of 29.21% when making the *n*-layer of 16-nm, intrinsic layer (*i*-layer) of 0.5-μm and *p*-layer of the 3-μm thickness with specific doping concentrations. We have found that by doping the *n*-layer with dopant of $1\cdot10^{20}$ cm^{-3}, *i*-layer with unintentionally doping concentration of $1.5\cdot10^{15}$ cm^{-3} and *p*-layer doping with $1\cdot10^{18}$ cm^{-3}, overall efficiency of 29.21% can be achieved. It is quite remarkable that the open circuit voltage, short circuit current density and percentage of fill factor values of the above mentioned solar cell structure are as follows: 1.0 V, 33.15 mA/cm^2 and 88.03%, respectively, by using Ni as metal contact. The dislocation density in the intrinsic layer plays a vital role in overall performance, as it should be less than or equal to $1\cdot10^{14}$ cm^{-3}, and the *i*-layer should be doped with acceptor type dopant to make the overall *n*-type unintentional doping (UID) concentration less than or equal to $1.5\cdot10^{16}$ cm^{-3}, to achieve the maximum efficiency from the solar cell structure.

References

1. Vurgaftman I. & Meyer J.R. Band parameters for nitrogen-containing semiconductors. *J. Appl. Phys.* 2003. **94**. P. 3675–3696. https://doi.org/10.1063/1.1600519.
2. Nakamura S. III–V nitride based light-emitting devices. *Solid State Commun*. 1997. **102**. P. 237–248. https://doi.org/10.1016/S0038-1098(96)00722-3.
3. Routray S.R. & Lenka T.R. InGaN-based solar cells: a wide solar spectrum harvesting technology for twenty-first century. *CSI Trans. ICT.* 2018. **6**. P. 83–96. https://doi.org/10.1007/s40012-017-0181-9.
4. Farahmand M. Garetto C., Bellotti E. *et al.* Monte Carlo simulation of electron transport in the III-nitride wurtzite phase materials system: binaries and ternaries. *IEEE Trans. Electron Devices.* 2001. **48**. P. 535–542. https://doi.org/10.1109/16.906448.
5. Hoshino T. & Mori N. Electron mobility calculation for two-dimensional electron gas in InN/GaN digital alloy channel high electron mobility transistors. *Jpn. J. Appl. Phys.* 2019. **58**. SCCD10. https://doi.org/10.7567/1347-4065/ab0409.
6. Askari M., Abadi V.M.M., Mirhabibi M. Types of solar cells and application. *Amer. J. Opt. Photon.* 2015. **3**. P. 94–113. https://doi.org/10.11648/j.ajop.20150305.17.
7. Rao S., Morankar A., Verma H., Goswami P. Emerging photovoltaics: Organic, copper zinc tin sulphide, and perovskite-based solar cells. *J. Appl. Chem.* 2016. **2016**. Article ID 3971579. https://doi.org/10.1155/2016/3971579.
8. Huang X., Li W., Fu H. *et al.* High-temperature polarization-free III-nitride solar cells with self-cooling effects. *ACS Photonics.* 2019. **6**. P. 2096–2103. https://doi.org/10.1021/acsphotonics.9b00655.
9. Yeh M.-Y., Lei P.-H., Lin S.-H., Yang C.-D. Copper-zinc-tin-sulfur thin film using spin-coating technology. *Materials.* 2016. **9**. P. 526. https://doi.org/10.3390/ma9070526.
10. Cho H.K., Lee J.Y., Yang G.M., Kim C.S. Formation mechanism of V defects in the InGaN/GaN multiple quantum wells grown on GaN layers with low threading dislocation density. *Appl. Phys. Lett.* 2001. **79**. P. 215–217. https://doi.org/10.1063/1.1384906.
11. Cho H.K., Lee J.Y., Kim C.S., Yang G.M. Influence of strain relaxation on structural and optical characteristics of InGaN/GaN multiple quantum wells with high indium composition. *J. Appl. Phys.* 2002. **91**. P. 1166–1170. https://doi.org/10.1063/1.1429765.

12. Cherns D., Henley S.J., Ponce F. Edge and screw dislocations as nonradiative centers in InGaN/GaN quantum well luminescence. *Appl. Phys. Lett.* 2001. **78**. P. 2691–2693. https://doi.org/10.1063/1.1369610.
13. Bernardini F., Fiorentini V., Vanderbilt D. Spontaneous polarization and piezoelectric constants of III-V nitrides. *Phys. Rev. B.* 1997. **56**. P. R10024–R10027. https://doi.org/10.1103/PhysRevB.56.R10024.
14. Chang, J.-Y. & Kuo, Y.-K. Simulation of N-face InGaN-based *p-i-n* solar cells. *J. Appl. Phys.* 2012. **112**. P. 033109. https://doi.org/10.1063/1.4745043.
15. Chang J.-Y., Liou B.-T., Lin H.-W. *et al.* Numerical investigation on the enhanced carrier collection efficiency of Ga-face GaN/InGaN *p-i-n* solar cells with polarization compensation interlayers. *Opt. Lett.* 2011. **36**. P. 3500–3502. https://doi.org/10.1364/ol.36.003500.
16. Li Y., You S., Zhu M. *et al.* Defect-reduced green GaInN/GaN light-emitting diode on nanopatterned sapphire. *Appl. Phys. Lett.* 2011. **98**. P. 151102. https://doi.org/10.1063/1.3579255.
17. Dahal R., Pantha B., Li J., Lin J.Y., Jiang H.X. InGaN/GaN multiple quantum well solar cells with long operating wavelengths. *Appl. Phys. Lett.* 2009. **94**. P. 063505. https://doi.org/10.1063/1.3081123.
18. Yang C.C., Sheu J.K., Liang Xin-Wei *et al.* Enhancement of the conversion efficiency of GaN-based photovoltaic devices with AlGaN/InGaN absorption layers. *Appl. Phys. Lett.* 2010. **97**. P. 021113. https://doi.org/10.1063/1.3463469.
19. Barnett A., Kirkpatrick D., Honsberg C. *et al.* Very high efficiency solar cell modules. *Progress in Photovoltaics.* 2009. **17**. P. 75–83. https://doi.org/10.1002/pip.852.
20. Toledo N.G., Friedman D.J., Farrell R.M. *et al.* Design of integrated III-nitride/non-III-nitride tandem photovoltaic devices. *J. Appl. Phys.* 2012. **111**. P. 054503. https://doi.org/10.1063/1.3690907.
21. Movla H., Salami D., Sadreddini S.V. Simulation analysis of the effects of defect density on the performance of *p-i-n* InGaN solar cell. *Appl. Phys. A.* 2012. **109**. P. 497–502. https://doi.org/10.1007/s00339-012-7062-8.
22. Chen X., Matthews K.D., Hao D. *et al.* Growth, fabrication, and characterization of InGaN solar cells. *phys. status solidi (a).* 2008. **205**. P. 1103–1105. https://doi.org/10.1002/pssa.200778695.
23. Valdueza-Felip S., Ajay A., Redaelli L. *et al. P-i-n* InGaN homojunctions (10–40% In) synthesized by plasma-assisted molecular beam epitaxy with extended photoresponse to 600 nm. *Solar Energy Materials and Solar Cells.* 2016. **160**. P. 355–360. https://doi.org/10.1016/j.solmat.2016.10.007.
24. Cai X.-M., Zeng S.-W., Zhang B.-P. Fabrication and characterization of InGaN *p-i-n* homojunction solar cell. *Appl. Phys. Lett.* 2009. **95**. P. 173504. https://doi.org/10.1063/1.3254215.
25. Niemegeers A., Burgelman M., Decock K. *et al. Simulation programme SCAPS-1D for thin film solar cells.* Department of Electronics and Information Systems (ELIS) of the University of Gent, Belgium, 2020. http://scaps.elis.ugent.be/.
26. Piprek J. *Semiconductor Optoelectronic Device: Introduction to Physics and Simulation*. Academic Press, 2003. P. 61–66.
27. Fabien C.A.M., Doolittle W.A. Guidelines and limitations for the design of high-efficiency InGaN single-junction solar cells. *Solar Energy Materials and Solar Cells.* 2014. **130**. P. 354–363. https://doi.org/10.1016/j.solmat.2014.07.018.
28. Hsu L., Walukiewicz W. Modeling of InGaN/Si tandem solar cells. *J. Appl. Phys.* 2008. **104**. P. 024507. https://doi.org/10.1063/1.2952031.
29. Shen Y.C., Mueller G.O., Watanabe S. *et al.* Auger recombination in InGaN measured by photoluminescence. *Appl. Phys. Lett.* 2007. **91**. P. 141101. https://doi.org/10.1063/1.2785135.
30. Van de Walle C.G. & Neugebauer J. First-principles calculations for defects and impurities: Applications to III-nitrides. *J. Appl. Phys.* 2004. **95**. P. 3851–3879. https://doi.org/10.1063/1.1682673.

Authors and CV

Sakhawat Hussain
He is working as an Associate Professor at the Department of Electrical and Electronic Engineering, University of Dhaka, Bangladesh. He has completed his Ph.D. from University of Nice Sophia Antipolis (UNS), France in 2014. His research interests are in semiconductor physics, optoelectronics, and material science, especially in group III-nitride materials.

Md. Mamunur Rahman
He is a final year undergraduate student at the Department of Electrical and Electronic Engineering, University of Dhaka, Bangladesh. His passion is to be an active researcher in his field of interest. His research interests are in material science, optoelectronics and nanoscale devices.
E-mail: *abirmamunurrahman@gmail.com*

Md. Tasrif Prodhan
He is in his final year undergraduate studies at the Department of Electrical and Electronic Engineering, University of Dhaka, Bangladesh. His research interests are in optoelectronic devices, especially light emitting diodes, lasers and solar cell devices. He is aimed to do his graduate and post-graduate studies in any of these fields of interest.
E-mail: *tasrifprodhan10@gmail.com*

Аналіз модельних характеристик для оптимізації сонячного елемента на основі $In_{0.7}Ga_{0.3}N$ з *p-i-n* гомопереходом

S. Hussain, Md. T. Prodhan and Md. M. Rahman

Анотація. Для визначення ідеальних структурних параметрів сонячного елемента на основі $In_{0.7}Ga_{0.3}N$ з *p-i-n* гомопереходом проведено моделювання, щоб отримати максимальну загальну ефективність. Показано, що параметри – *n*-шар товщиною 16 нм, власний шар (*i*-шар) товщиною 0,5 мкм і *p*-шар товщиною 3 мкм з відповідними концентраціями легування $1\cdot10^{20}$ см$^{-3}$ для *n*-шару і $1\cdot10^{18}$ см$^{-3}$ для *p*-шару – дозволяють досягти максимальної ефективності 29,21%. Конструкція сонячного елемента забезпечує напругу холостого ходу 1,0 В, густину струму короткого замикання 33,15 мА/см^2 і коефіцієнт заповнення 88,03%. Однак ефективність різко падає, якщо щільність дислокацій в *i*-шарі більше ніж $1\cdot10^{14}$ см$^{-3}$, а фонова концентрація домішок в *i*-шарі перевищує $1{,}5\cdot10^{16}$ см$^{-3}$.

Ключові слова: *p-i-n* гомоперехід, сонячний елемент, пристрій для моделювання ємності сонячних елементів (SCAPS).